Pre-Disaster Allocation of Mobile Renewable-Powered Resilience-Delivery Sources in Power Distribution Networks

Jinshun Su*, Ruotan Zhang†, Payman Dehghanian‡
Department of Electrical and Computer Engineering
The George Washington University
Washington, DC, USA.
{*jsu66, †zhangruotan114, ‡payman}@gwu.edu

Mohammad Heidari Kapourchali
Department of Electrical Engineering
University of Alaska Anchorage
Anchorage, AK, USA.
mhkapourchali@alaska.edu

***Abstract*—Unlike stationary wind turbines, mobile wind turbines (MWTs) can travel along the local transportation system (TS) via a truck, supplying power to microgrids (MGs), residential buildings, and critical infrastructure. This spatiotemporal flexibility can provide significant benefits, including enhancing system resilience in the aftermath of high-impact low-probability (HILP) incidents. However, the potential of such resources is currently untapped, calling for improved utilization. To address this research gap, this paper proposes an optimal scheme for strategically pre-positioning MWTs to enhance the resilience of MGs when facing extreme events. Considering that the MWTs travel time on the TS and the predicted wind energy have a significant impact on the duration and magnitude of power outages during the restoration process, a scenario-based stochastic mixed-integer linear programming (MILP) model is introduced to incorporate uncertainties related to the road status in the TS, power line faults in MGs, and wind energy forecasts. Case studies on an integrated transportation and energy network — a central Alabama interstate transportation network and two IEEE 33-node test power systems — demonstrate the effectiveness of the proposed pre-positioning scheme in boosting MGs resilience.**

***Index Terms*—Mobile wind turbine (MWT), pre-positioning, resilience, mixed-integer linear programming (MILP), scenarios, stochastic programming.**

NOMENCLATURE

A. Sets

$\mathbf{M}$	Set of mobile wind turbines (MWTs).
$\mathbf{K}$	Set of nodes in the transportation system (TS).
$\mathbf{T}$	Set of time periods in the decision-making horizon.
$\mathbf{\Phi}$	Set of microgrids (MGs).
$\mathbf{I}_\phi$	Set of nodes in the MG ϕ.
$\mathbf{I}_\phi^c \subset \mathbf{I}_\phi$	Set of candidate nodes in the MG ϕ.
$\mathbf{K}^d \subset \mathbf{K}$	Set of TS nodes where depots are located.
$\mathbf{S}$	Set of scenarios.
$\mathbf{L}_\phi$	Set of power lines in the MG ϕ.
$\mathbf{H}$	Set of hydrogen storage systems (HSSs).

B. Parameters

C_k	Maximum number of MWTs allowed to be connected to TS node k.
$\Lambda_{k\phi i}$	Indicator denoting whether TS node k is mapped to candidate node i of MG ϕ.
$a_{\phi i}$	Interrupted energy assessment rate for node i of MG ϕ.
$b_{\phi t}$	Price of undelivered energy from the electric utility of MG ϕ at time t.
$P^D_{\phi it}, Q^D_{\phi it}$	Real/Reactive power demand in node i of MG ϕ at time t.
P^G_ϕ, Q^G_ϕ	Real/Reactive power capacity of substation at MG ϕ.
$\underline{\theta}_{\phi i}, \overline{\theta}_{\phi i}$	Lower/Upper bounds of power factor angle at node i of MG ϕ.
$P^F_{\phi l}, Q^F_{\phi l}$	Real/Reactive power flow capacity of line l of MG ϕ.
U	Big M number.
$R_{\phi l}, X_{\phi l}$	Resistance/Reactance of line l of MG ϕ.
$\underline{V}^{sq}_{\phi i}, \overline{V}^{sq}_{\phi i}$	Minimum/Maximum squared voltage magnitude at node i of MG ϕ.
$\rho_{h\phi i}$	Indicator denoting whether HSS h is located at node i of MG ϕ.
E^{ini}_h	Initial hydrogen storage level of HSS h.
$\underline{E}_h, \overline{E}_h$	Minimum/Maximum hydrogen storage level of HSS h.
$\eta^{p2h}_h, \eta^{h2p}_h$	Power-to-hydrogen (P2H)/Hydrogen-to-power (H2P) efficiency of HSS h.
$\overline{P}^{p2h}_h, \overline{P}^{h2p}_h$	Maximum capacity of consumed/generated power of HSS h in P2H/H2P mode.
W^{Cap}_m	Wind power capacity of MWT m.
π_s	Probability of scenario s.
$\omega_{k\hat{k}s}$	Realization of random variable denoting travel time from TS nodes k to $\hat{k}$ in scenario s.
$\lambda_{\phi lt}$	Realization of random variable denoting the status (on/off) of the power line l of MG ϕ at time t in scenario s.
$\xi_{\phi ts}$	Realization of random variable denoting the predicted wind energy at MG ϕ at time t in scenario s.

C. Decision Variables

x_{mk}	Binary variable indicating whether MWT m is pre-positioned at TS node k.

y_{mkts}	Binary variable indicating whether MWT m is assigned to TS node k at time t in scenario s.
$z_{m\phi its}$	Binary variable indicating whether MWT m is assigned to node i of MG ϕ at time t in scenarios s.
$p^{out}_{\phi its}, q^{out}_{\phi its}$	Real/Reactive power outage in node i of MG ϕ at time t in scenario s.
$\psi_{m\phi its}$	Power injection from individual MWT m to node i of MG ϕ at time t in scenario s.
$p^{w}_{\phi its}$	Total power injection from all possible MWTs to node i of MG ϕ at time t in scenario s.
$v^{sq}_{\phi its}$	Squared voltage magnitude at node i of MG ϕ at time t in scenario s.
$p^{g}_{\phi its}, q^{g}_{\phi its}$	Total real/reactive power injection to node i of MG ϕ at time t in scenario s.
$p^{f}_{\phi lts}, q^{f}_{\phi lts}$	Real/Reactive power flow in line l of MG ϕ at time t in scenario s.
$\mu^{p2h}_{hts}, \mu^{h2p}_{hts}$	Binary variable indicating whether HSS h is in P2H/H2P mode at time t in scenario s.
$p^{p2h}_{hts}, p^{h2p}_{hts}$	Consumed/Generated power of HSS h in P2H/H2P mode at time t in scenario s.
E_{hts}	Hydrogen storage level of HSS h at time t in scenario s.
p^{net}_{hts}	The net power output of HSS h at time t in scenario s.

I. Introduction

Climate change is driving global warming, resulting in a growing prevalence of high-impact low-probability (HILP) events on a global scale. Such HILP incidents – e.g., hurricanes, wildfires, winter storms – have led to excessive equipment damages, prolonged electricity outages, significant economic losses, and disruptions in our modern society [1]. Figure 1 demonstrates the increasing frequency of billion-dollar disasters in the United States from 1980 to 2021 [2], most of which resulted in extensive electricity outages. For example, in February 2021, an extreme winter storm caused a massive electricity generation failure in Texas, which led to more than 4.5 million households without electricity at its peak for several days and approximately $130 billion in economic losses [3]. Power outages triggered by climate change have inflicted substantial economic losses and posed significant threats to human life, underscoring the critical need for improving power grid resilience [4].

The development of sustainable energy systems is observed as imperative to mitigate the impacts of climate change-driven HILP incidents. In response to these environmental concerns, renewable and clean energy resources have been widely adopted and integrated into modern power systems [5]–[8]. The rapid deployment of distributed energy resources can significantly reduce carbon emissions and enhance the resilience of the power grid in the face of extreme events [9]. For instance, the study [10] develops an adaptive robust optimization model to facilitate a faster and more reliable self-healing process by coordinating wind farms and pumped-storage hydro units. Additionally, study [11] presents an

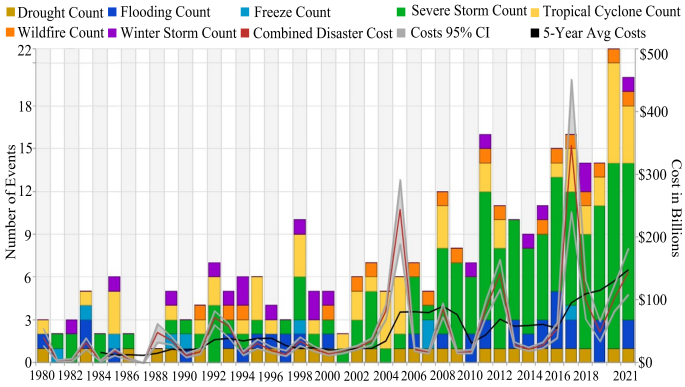

Fig. 1. United States billion-dollar disaster events from 1980-2021 [2].

effective restoration strategy that incorporates wind energy participation, aiming to achieve an elevated level of grid resilience in the face of widespread emergencies.

Compared to stationary renewable energy resources, such as solar panels, wind turbines, and hydrogen storage systems (HSSs), the utilization of mobile power sources (MPSs) holds significant promise for enabling spatiotemporal flexibility exchange within MGs and has garnered growing interest due to its potential to enhance system resilience and improve overall system efficiency. For instance, a joint post-disaster restoration scheme applying MPSs and distributed generators tackling the transportation system (TS) constraints is proposed in [12]. Considering the integration of the MPSs and repair crews' dispatch, the study in [13] proposes a co-optimization approach formulated as a mixed-integer second-order cone programming model for distribution system resilience. The study in [14] proposes a two-stage restoration scheme for distribution system restoration capturing the full potential of MPSs dispatch jointly with the dynamic distribution system reconfiguration under a suite of seismic force scenarios. The study in [15] develops a novel restoration mechanism in distribution systems for deployment of MPSs integrated with stochastic renewable energy sources, capturing the uncertainty of renewable energy sources with joint probabilistic constraints. The study in [16] considers decision-dependent uncertainty in the availability of MPSs due to travel and waiting times for offering a more realistic estimation of the MPSs' contributions to distribution system resilience enhancement. Achieved by the strategic deployment of MPSs, the study in [17] proposes a risk-averse model to generate a public-safety power-shutoff plan for balancing wildfire risks and power outages.

However, MPSs investigated in the literature [12]–[17] consume traditional energy to supply power, which have higher operating costs and yield harmful emissions. Mobile wind turbines (MWTs) are small-scale wind turbines that are designed to be easily transportable and commonly used for off-grid power generation or to power remote locations. The study [18] incorporates joint utilization of MWTs and electric thermal storage into the MG energy portfolio, which can shift the load profile and prevent costs associated with peak demand. Enabling spatiotemporal flexibility, MWTs can serve as an exceptional choice for providing emergency power

to damaged power systems in the face of extreme weather.

To the best of our knowledge, the existing literature lacks analytical models for MWTs allocation (i.e., pre-positioning) for service restoration in rural locations. To fill in this knowledge gap, we develop a novel restoration scheme that integrates the pre-positioning of MWTs and the operation of HSSs in rural MGs. The proposed model is formulated as a scenario-based stochastic mixed-integer linear programming (MILP) model to capture uncertainties in the road status of the TS, power line faults in MGs, and predicted wind energy. The model performance is verified on an integrated test system: a central Alabama interstate transportation network and two IEEE 33-node test power systems.

The rest of the paper is organized as follows: Section II introduces the proposed MWTs pre-positioning model. Section III describes the method for scenario generation. Section IV discusses numerical results, and Section V summarizes the research findings.

II. Problem Formulation

In this section, we introduce a novel service restoration model that takes into consideration the pre-positioning of MWTs in the face of uncertain road status in the TS, power line faults in MGs, and predicted wind energy. The proposed model is formulated as a scenario-based MILP problem with the following objective function:

$$\min \sum_{s\in\mathbf{S}} \pi_s \sum_{\phi\in\mathbf{\Phi}} \sum_{i\in\mathbf{I}_\phi} \sum_{t\in\mathbf{T}} (a_{\phi i} + b_{\phi t}) p^{out}_{\phi its} \tag{1}$$

The objective function (1) aims to minimize the expected costs of power outages including the interruption cost imposed to customers (i.e., $a_{\phi i}p^{out}_{\phi its}$) and the revenue-loss imposed to the electric utility (i.e., $b_{\phi t}p^{out}_{\phi its}$). The proposed optimization model has a mixed-integer linear feasible set defined by the constraints described in the following subsections II-A –II-E. To ease the notations, we define index sets $\mathbf{\Omega} = \{(m,k,\phi,i,t) : m\in\mathbf{M}, k\in\mathbf{K}, \phi\in\mathbf{\Phi}, i\in\mathbf{I}^c_\phi, t\in\mathbf{T}, s\in\mathbf{S}\}$, and $\tilde{\mathbf{\Omega}} = \{(\phi,t,s) : \phi\in\mathbf{\Phi}, t\in\mathbf{T}, s\in\mathbf{S}\}$.

A. MWTs Pre-positioning and Allocation Constraints

Constraint (2a) enforces a capacity limit on the number of MWTs that can be pre-positioned at each depot. Constraint (2b) ensures that each MWT is pre-positioned to exactly one of the depots. Constraint (2c) ensures the initial location of MWT m prior to its deployment in scenario s. The routing and scheduling of MWTs in scenario s are defined by constraint (2d). Constraint (2e) stipulates that the total number of MWTs located at TS node k at any time period does not exceed the maximum number of vehicles that node k can host. Each MWT m can stay in at most one node at any time period as enforced by constraint (2f). There exists a correspondence between MG candidate nodes and TS nodes, hereafter called *coupling points/nodes* [1]. Constraint (2g) ensures that MG candidate node i can be served by MWT m only if it reaches coupling node k of the TS at time t in scenario s.

$$\sum_{m\in\mathbf{M}} x_{mk} \le C_k, \qquad \forall k\in\mathbf{K}^d \tag{2a}$$

$$\sum_{k\in\mathbf{K}^d} x_{mk} = 1, \qquad \forall m\in\mathbf{M} \tag{2b}$$

$$y_{mk1s} = x_{mk}, \qquad \forall m\in\mathbf{M}, k\in\mathbf{K}^d, s\in\mathbf{S} \tag{2c}$$

$$y_{mk(t+\tau)s} \le 1 - y_{m\hat{k}ts}, \quad \forall m\in\mathbf{M}, k,\hat{k}\in\mathbf{K}, \tau\le\omega_{k\hat{k}s}, t\le|\mathbf{T}|-\tau, s\in\mathbf{S} \tag{2d}$$

$$\sum_{m\in\mathbf{M}} y_{mkts} \le C_k, \qquad \forall k\in\mathbf{K}, t\in\mathbf{T}, s\in\mathbf{S} \tag{2e}$$

$$\sum_{k\in\mathbf{K}} y_{mkts} \le 1, \qquad \forall m\in\mathbf{M}, t\in\mathbf{T}, s\in\mathbf{S} \tag{2f}$$

$$y_{mkts} \ge \Lambda_{k\phi i} z_{m\phi its}, \qquad \forall k\in\mathbf{K}, (m,\phi,i,t,s)\in\mathbf{\Omega} \tag{2g}$$

B. MWTs Operation Constraints

Constraint (3a) ensures that the power output of MWT m does not exceed its capacity if it is connected. Constraint (3b) denotes that the total power output of MWTs cannot be greater than the predicted wind energy in MG ϕ at time t. Constraints (3c) and (3d) stipulate the total power injection from all possible MWTs to each candidate node of MGs.

$$0 \le \psi_{m\phi its} \le W^{Cap}_m z_{m\phi its}, \qquad \forall (m,\phi,i,t,s)\in\mathbf{\Omega} \tag{3a}$$

$$\sum_{m\in\mathbf{M}} \psi_{m\phi its} \le \xi_{\phi ts}, \qquad \forall (m,\phi,i,t,s)\in\mathbf{\Omega} \tag{3b}$$

$$p^w_{\phi its} = \sum_{m\in\mathbf{M}} \psi_{m\phi its}, \qquad \forall (m,\phi,i,t,s)\in\mathbf{\Omega} \tag{3c}$$

$$p^w_{\phi its} = 0, \qquad \forall i\in\mathbf{I}^c_\phi\setminus\mathbf{I}_\phi, (\phi,t,s)\in\tilde{\mathbf{\Omega}} \tag{3d}$$

C. MGs Power Balance Constraints

Constraints (4a) and (4b) denote the real and reactive power balance conditions at each node in each MG. The notations $\Theta(l)$ and $\Gamma(l)$ represent the source and terminal nodes of power line l, respectively. Constraints (4c) and (4d) ensure the limits for real and reactive power outages at each node. Constraints (4e) and (4f) represent boundaries of real and reactive power injection at the substation node (i.e., node 1) of each MG. The real and reactive power injection at non-substation nodes is set by constraints (4g) and (4h).

$$\sum_{l\in\mathbf{L}_\phi;\Theta(l)=i} p^f_{\phi lts} - \sum_{l\in\mathbf{L}_\phi;\Gamma(l)=i} p^f_{\phi lts} = p^g_{\phi its} - (P^D_{\phi it} - p^{out}_{\phi its}), \quad \forall i\in\mathbf{I}_\phi, (\phi,t,s)\in\tilde{\mathbf{\Omega}} \tag{4a}$$

$$\sum_{l\in\mathbf{L}_\phi;\Theta(l)=i} q^f_{\phi lts} - \sum_{l\in\mathbf{L}_\phi;\Gamma(l)=i} q^f_{\phi lts} = q^g_{\phi its} - (Q^D_{\phi it} - q^{out}_{\phi its}), \quad \forall i\in\mathbf{I}_\phi, (\phi,t,s)\in\tilde{\mathbf{\Omega}} \tag{4b}$$

$$0 \le p^{out}_{\phi its} \le P^D_{\phi it}, \qquad \forall i\in\mathbf{I}_\phi, (\phi,t,s)\in\tilde{\mathbf{\Omega}} \tag{4c}$$

$$0 \le q^{out}_{\phi its} \le Q^D_{\phi it}, \qquad \forall i\in\mathbf{I}_\phi, (\phi,t,s)\in\tilde{\mathbf{\Omega}} \tag{4d}$$

$$0 \le p^g_{\phi 1ts} \le P^G_\phi, \qquad \forall (\phi,t,s)\in\tilde{\mathbf{\Omega}} \tag{4e}$$

$$0 \le q^g_{\phi 1ts} \le Q^G_\phi, \qquad \forall (\phi,t,s)\in\tilde{\mathbf{\Omega}} \tag{4f}$$

$$p^g_{\phi its} = \sum_{h\in\mathbf{H}} \rho_{h\phi i} p^{net}_{hts} + p^w_{\phi its}, \quad \forall i\in\mathbf{I}^c_\phi\setminus\{1\}, (\phi,t,s)\in\tilde{\mathbf{\Omega}} \tag{4g}$$

$$p^g_{\phi its}\tan\underline{\theta}_{\phi i} \le q^g_{\phi its} \le p^g_{\phi its}\tan\overline{\theta}_{\phi i}, \quad \forall i \in \mathbf{I}^c_\phi \setminus \{1\}, (\phi,t,s) \in \tilde{\mathbf{\Omega}} \quad (4h)$$

D. MGs Power Flow Constraints

Constraints (5a) and (5b) represent the power flow equations considering the status of power lines where the term $U(1-\lambda_{\phi lts})$ or $U(\lambda_{\phi lts}-1)$ ensures that the power flow condition is satisfied for connected lines [19]. The real and reactive power flow in online lines are limited by their active and reactive capacities in constraints (5c) and (5d), separately.

$$v^{sq}_{\phi its} - v^{sq}_{\phi jts} \le \frac{2(R_{\phi l}p^f_{\phi lts} + X_{\phi l}q^f_{\phi lts})}{1000} + U(1-\lambda_{\phi lts}), \quad \forall i,j \in \mathbf{I}_\phi, l \in \mathbf{L}_\phi, (\phi,t,s) \in \tilde{\mathbf{\Omega}} \quad (5a)$$

$$v^{sq}_{\phi its} - v^{sq}_{\phi jts} \ge \frac{2(R_{\phi l}p^f_{\phi lts} + X_{\phi l}q^f_{\phi lts})}{1000} + U(\lambda_{\phi lts}-1), \quad \forall i,j \in \mathbf{I}_\phi, l \in \mathbf{L}_\phi, (\phi,t,s) \in \tilde{\mathbf{\Omega}} \quad (5b)$$

$$-P^F_{\phi l}\lambda_{\phi lts} \le p^f_{\phi lts} \le P^F_{\phi l}\lambda_{\phi lts}, \ \forall l \in \mathbf{L}_\phi, (\phi,t,s) \in \tilde{\mathbf{\Omega}} \quad (5c)$$

$$-Q^F_{\phi l}\lambda_{\phi lts} \le q^f_{\phi lts} \le Q^F_{\phi l}\lambda_{\phi lts}, \forall l \in \mathbf{L}_\phi, (\phi,t,s) \in \tilde{\mathbf{\Omega}} \quad (5d)$$

E. HSSs Operation Constraints

The variations in the hydrogen storage level of HSS h over time is determined by their power-to-hydrogen (P2H) and hydrogen-to-power (H2P) behaviors, as denoted in constraint (6a). Constraint (6b) defines the initial hydrogen storage level setting of HSS h. Constraint (6c) specifies the range of the hydrogen storage level of HSS h. Constraints (6d) and (6e) represent output boundaries of HSS h in P2H and H2P modes, respectively. Constraint (6f) indicates that P2H and H2P modes of HSS h are mutually exclusive. Constraint (6g) restricts the net real power output of HSS h.

$$E_{h(t+1)s} = E_{hts} + \left(p^{p2h}_{hts}\eta^{p2h}_h - \frac{p^{h2p}_{hts}}{\eta^{h2p}_h}\right), \quad \forall h \in \mathbf{H}, t \in \mathbf{T} \setminus \{|\mathbf{T}|\}, s \in \mathbf{S} \quad (6a)$$

$$E_{h1s} = E^{ini}_h, \quad \forall h \in \mathbf{H}, s \in \mathbf{S} \quad (6b)$$

$$\underline{E}_h \le E_{hts} \le \overline{E}_h, \quad \forall h \in \mathbf{H}, t \in \mathbf{T}, s \in \mathbf{S} \quad (6c)$$

$$0 \le p^{p2h}_{hts} \le \overline{P}^{p2h}_h \mu^{p2h}_{hts}, \quad \forall h \in \mathbf{H}, t \in \mathbf{T}, s \in \mathbf{S} \quad (6d)$$

$$0 \le p^{h2p}_{hts} \le \overline{P}^{h2p}_h \mu^{h2p}_{hts}, \quad \forall h \in \mathbf{H}, t \in \mathbf{T}, s \in \mathbf{S} \quad (6e)$$

$$\mu^{p2h}_{hts} + \mu^{h2p}_{hts} \le 1, \quad \forall h \in \mathbf{H}, t \in \mathbf{T}, s \in \mathbf{S} \quad (6f)$$

$$p^{net}_{hts} = p^{h2p}_{hts} - p^{p2h}_{hts} \quad \forall h \in \mathbf{H}, t \in \mathbf{T}, s \in \mathbf{S} \quad (6g)$$

III. Scenario Generations

Uncertainties arise on the road conditions of the TS, faults in power lines within MGs, and wind energy predictions. In this study, we use Monte Carlo simulation to generate a multitude of scenarios to capture the various realizations of random variables, such as travel time between nodes in the TS, the status of power lines in MGs, and the availability of wind energy around MGs.

Note that the statuses of roads in TS and power lines in MGs are classified as either survival or failure in the event of a HILP event. By employing the binomial distribution, we derive the initial statuses of roads and power lines in different scenarios. To determine the travel time between nodes in the TS ($\omega_{k\hat{k}s}$), we coordinate the initial status of roads with a shortest-path algorithm [20]. Additionally, assuming that broken power lines in MGs are repaired within a fixed timeframe, we establish the status of power lines during each time period ($\lambda_{\phi ls}$). The accurate prediction of wind energy production relies heavily on modeling wind speed. In this context, the Weibull distribution is commonly employed because of its capability to capture uncorrelated wind speeds [21], [22]. By utilizing the Weibull distribution, one can derive the potential wind power outputs in different scenarios ($\xi_{\phi ts}$).

Monte Carlo simulation generates a large number of scenarios to capture the realizations of random variables. To mitigate computational complexity, we employ the Backward Scenario Reduction algorithm [23], which allows us to reduce the number of scenarios to a tractable size.

IV. Numerical Results

A. Test System Description

In this section, the effectiveness of the proposed model is verified by application to a test case that integrates a TS and multiple MGs — a central Alabama interstate transportation network [24] and two IEEE 33-node test power systems [19]. The configuration of the test system is illustrated in Fig. 2, where MGs and TS networks are integrated through several coupling nodes defined in Table I. Detailed information on HSSs can be found in [25]. Six MWTs are considered in the test system, each with 300 kW capacity, while 3 depots — which are located in nodes 10, 13, and 19, respectively — are taken into account. The entire restoration time horizon in all conducted tests is assumed to be 24 periods of 30-minute duration (i.e. 12 hours). We investigated the impact of jointly implementing MWTs and HSSs on power system resilience by studying three different cases on the introduced test system: ***Case I*** includes neither MWTs nor HSSs; ***Case II*** considers MWTs dispatch without the presence of HSSs; ***Case III*** involves the participation of both MWTs and HSSs in service restoration. Numerical tests are conducted on a machine with an Intel i7-8700 processor and 32 GB RAM. The optimization problem is formulated with AMPL and solved with the optimization solver Gurobi 10.0.0.

TABLE I
Coupling Points in the Integrated Test System of a TS and Multiple MGs

TS	MG1	TS	MG2
1	n16	14	n2
2	n13	18	n3
3	n30	20	n25
4	n8	21	n20
5	n5	22	n6
6	n2	23	n28
7	n24	24	n18
8	n21	25	n12
9	n27	26	n9
		27	n32

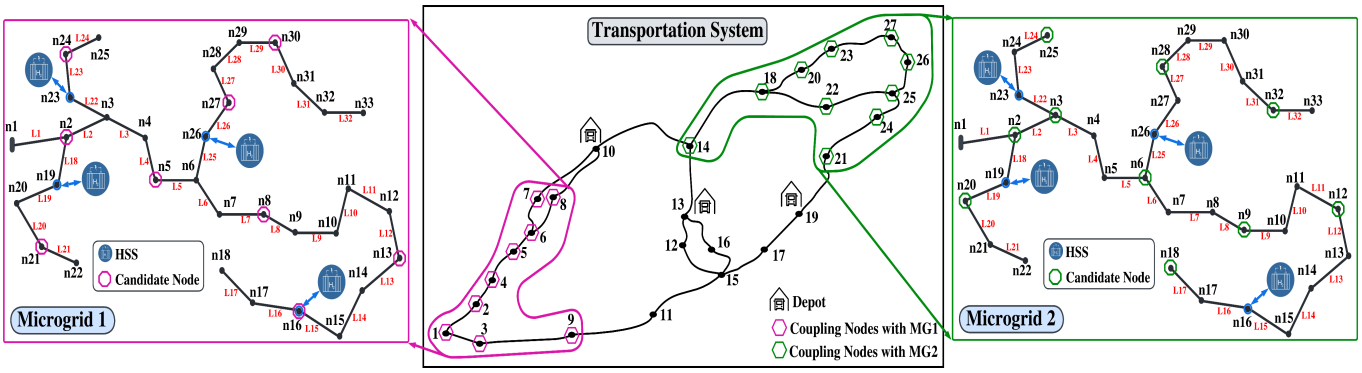

Fig. 2. An integrated test system with a central Alabama interstate transportation network and four MGs.

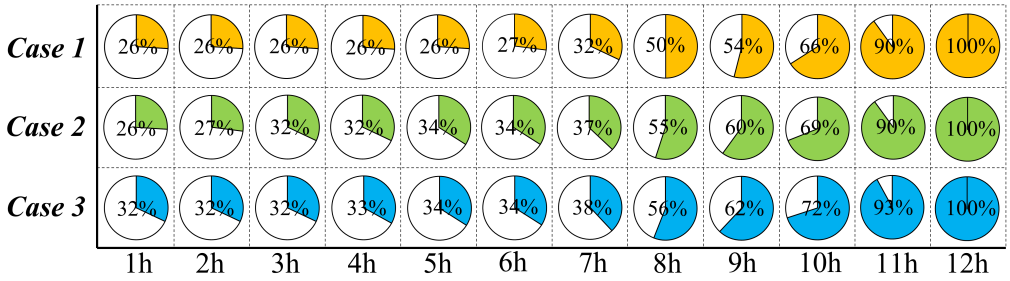

Fig. 3. Percentage of the total restored demand over time under different studied cases.

B. Analysis and Discussions

Figure 3 illustrates the percentage of restored demand across multiple MGs under different cases. When comparing the values found in ***Case I*** and ***Case II***, it is evident that the utilization of MWTs results in a higher percentage of restored demand during the early time periods of the restoration process (i.e., 26% versus 32% within 3 hours). Furthermore, in ***Case III***, where HSSs are introduced, a greater amount of the power outage can be restored within the first hour of the restoration process compared to ***Case I*** and ***Case II*** (i.e., 26% in ***Case I*** and ***Case II***, 32% in ***Case III***). Throughout the duration of 1 hour to 11 hours, ***Case III*** consistently exhibits a higher percentage of total restored demand compared to ***Case I*** in each time period, highlighting that the integration of MWTs and HSSs into the restoration process enables a quicker and more efficient recovery from power outages.

Table II provides an overview of the results for all investigated cases. Analyzing the findings presented in Table II, several key insights can be highlighted: (i) The transition from ***Case I*** to ***Case II*** demonstrates a reduction in the total power outage costs, showcasing the potential of MWTs and HSSs to lower outage-related expenses and enhance the resilience of MGs; (ii) Introducing HSSs into the scenarios where MWTs are deployed leads to a reduction in wind curtailment, with the percentage dropping from 42.52% to 36.16%. This outcome highlights the positive impact of coordinating MWTs with the operation of HSSs on boosting the resilience of communities and critical infrastructures while minimizing wind curtailment as much as possible.

Table III provides an overview of the decisions made regarding the pre-positioning and allocation of MWTs in the TS. Upon reviewing Table III, the following observations can

TABLE II
SUMMARY OF THE RESULTS IN ALL STUDIED CASES

Case	Outage Costs ($)	Wind Curtailment Percentage (%)
I	21,853k	100
II	20,163k	42.52
III	19,272k	34.16

be made: (i) Two MWTs are pre-positioned at the depot located at node 10 and subsequently assigned to nodes 6 and 7, respectively; (ii) One MWT is pre-positioned at the depot situated at node 13 and deployed to node 14; (iii) Three MWTs are pre-positioned at the depot located at node 19 and subsequently allocated to nodes 21, 27, and 25, separately.

TABLE III
OPTIMAL MWTS PRE-POSITIONING AND ALLOCATION DECISIONS IN THE TEST SYSTEM

Depot Location	Pre-positioning Decisions		Allocation Decisions
node 10	MWT1	→→	Allocated to node 6
	MWT2	→→	Allocated to node 7
node 13	MWT3	→→	Allocated to node 14
node 19	MWT4	→→	Allocated to node 21
	MWT5	→→	Allocated to node 27
	MWT6	→→	Allocated to node 25

Next, we assess the effectiveness of decarbonization through the utilization of MWTs by comparing it to the conventional approach of using mobile emergency generators (MEGs). Specifically, we investigate the performance of six MEGs with a capacity of 300 kW [1], using the same settings as in all studied cases. We estimate the carbon dioxide (CO_2)

emissions resulting from the use of MEGs during the restoration process based on the report by the U.S. Environmental Protection Agency [26]. Table IV presents a comparison of the CO_2 emissions and power outage costs resulting from the utilization of MWTs and MEGs. Our analysis reveals that, when compared to MEGs, MWTs can achieve a similar effort of reducing power outage costs, while offering the additional benefit of zero CO_2 emissions. This finding demonstrates the potential of MWTs in promoting sustainable power restoration processes, which are crucial in mitigating the negative impact of power outages on both environment and the society.

TABLE IV
PERFORMANCE COMPARISON OF THE PROPOSED MWTS VS. CONVENTIONAL MEGS

Types	**Outage Costs ($)**	CO_2 **Emissions** (ton)
MWTs	19,272k	0
MEGs	19,236k	3.04

V. CONCLUSION

In this paper, we developed a novel restoration scheme to enhance the resilience of MGs through optimal decisions on the pre-positioning of MWTs and their joint operation with HSSs. The proposed scheme was formulated as a scenario-based stochastic MILP model to capture uncertainties in the status of roads in the TS, power line faults in MGs, and wind energy predictions. Numerical results on an integrated transportation and energy network — a central Alabama interstate transportation network and two IEEE 33-node test power systems — highlighted the benefit and efficacy of the proposed approach in boosting MGs resilience against HILP extremes while achieving improved decarbonization goals.

VI. ACKNOWLEDGMENT

This work was supported in part by the U.S. National Science Foundation (NSF) under Grants RISE-2022505, RISE-2022705, RISE-2220624, RISE-2220626, and ECCS-2114100.

REFERENCES

[1] D. Anokhin, P. Dehghanian, M. A. Lejeune, and J. Su, "Mobility-as-a-service for resilience delivery in power distribution systems," *Production and Operations Management*, vol. 30, no. 8, pp. 2492–2521, 2021.

[2] A. B. Smith, "2021 U.S. billion-dollar weather and climate disasters in historical context," 2021. Available at https://www.climate.gov/news-features/blogs/beyond-data/2021-us-billion-dollar-weather-and-climate-disasters-historical.

[3] J. W. Busby, K. Baker, M. D. Bazilian, A. Q. Gilbert, E. Grubert, V. Rai, J. D. Rhodes, S. Shidore, C. A. Smith, and M. E. Webber, "Cascading risks: Understanding the 2021 winter blackout in Texas," *Energy Research & Social Science*, vol. 77, p. 102106, 2021.

[4] P. Dehghanian, B. Zhang, T. Dokic, and M. Kezunovic, "Predictive risk analytics for weather-resilient operation of electric power systems," *IEEE Transactions on Sustainable Energy*, vol. 10, no. 1, pp. 3–15, 2019.

[5] S. Wang, P. Dehghanian, M. Alhazmi, J. Su, and B. Shinde, "Resilience-assured protective control of DC/AC inverters under unbalanced and fault scenarios," in *2019 IEEE Power & Energy Society Innovative Smart Grid Technologies Conference (ISGT)*, pp. 1–5, 2019.

[6] L. He and J. Zhang, "A community sharing market with PV and energy storage: An adaptive bidding-based double-side auction mechanism," *IEEE Transactions on Smart Grid*, vol. 12, no. 3, pp. 2450–2461, 2021.

[7] N. Shi, Graduate, R. Cheng, L. Liu, Z. Wang, Q. Zhang, and M. J. Reno, "Data-driven affinely adjustable robust Volt/VAr control," *IEEE Transactions on Smart Grid*, pp. 1–1, 2023.

[8] P. Huang and L. Vanfretti, "Adaptive passivity compensation of grid-following MMC for stable grid integration," in *2022 IEEE Industry Applications Society Annual Meeting (IAS)*, pp. 1–8, 2022.

[9] X. Huo, J. Dong, B. Cui, B. Liu, J. Lian, and M. Liu, "Two-level decentralized-centralized control of distributed energy resources in grid-interactive efficient buildings," *IEEE Control Systems Letters*, vol. 7, pp. 997–1002, 2023.

[10] A. Golshani, W. Sun, Q. Zhou, Q. P. Zheng, J. Wang, and F. Qiu, "Coordination of wind farm and pumped-storage hydro for a self-healing power grid," *IEEE Transactions on Sustainable Energy*, vol. 9, no. 4, pp. 1910–1920, 2018.

[11] J. Su, P. Dehghanian, M. Nazemi, and B. Wang, "Distributed wind power resources for enhanced power grid resilience," in *2019 North American Power Symposium (NAPS)*, pp. 1–6, 2019.

[12] S. Yao, P. Wang, and T. Zhao, "Transportable energy storage for more resilient distribution systems with multiple microgrids," *IEEE Transactions on Smart Grid*, vol. 10, no. 3, pp. 3331–3341, 2018.

[13] S. Lei, C. Chen, Y. Li, and Y. Hou, "Resilient disaster recovery logistics of distribution systems: Co-optimize service restoration with repair crew and mobile power source dispatch," *IEEE Transactions on Smart Grid*, vol. 10, no. 6, pp. 6187–6202, 2019.

[14] Z. Yang, P. Dehghanian, and M. Nazemi, "Seismic-resilient electric power distribution systems: Harnessing the mobility of power sources," *IEEE Transactions on Industry Applications*, vol. 56, no. 3, pp. 2304–2313, 2020.

[15] M. Nazemi, P. Dehghanian, X. Lu, and C. Chen, "Uncertainty-aware deployment of mobile energy storage systems for distribution grid resilience," *IEEE Transactions on Smart Grid*, vol. 12, no. 4, pp. 3200–3214, 2021.

[16] J. Su, D. Anokhin, P. Dehghanian, and M. A. Lejeune, "On the use of mobile power sources in distribution networks under endogenous uncertainty," *IEEE Transactions on Control of Network Systems*, pp. 1–12, 2023.

[17] J. Su, S. Mehrani, P. Dehghanian, and M. A. Lejeune, "Quasi second-order stochastic dominance model for balancing wildfire risks and power outages due to proactive public safety de-energizations," *IEEE Transactions on Power Systems*, pp. 1–14, 2023.

[18] J. Su, P. Dehghanian, B. Vergara, and M. H. Kapourchali, "An energy management system for joint operation of small-scale wind turbines and electric thermal storage in isolated microgrids," in *2021 North American Power Symposium (NAPS)*, pp. 1–6, 2021.

[19] M. E. Baran and F. F. Wu, "Network reconfiguration in distribution systems for loss reduction and load balancing," *IEEE Power Engineering Review*, vol. 9, no. 4, pp. 101–102, 1989.

[20] K. Magzhan and H. M. Jani, "A review and evaluations of shortest path algorithms," *International journal of scientific & technology research*, vol. 2, no. 6, pp. 99–104, 2013.

[21] C. Ozay and M. S. Celiktas, "Statistical analysis of wind speed using two-parameter weibull distribution in Alaçatı region," *Energy Conversion and Management*, vol. 121, pp. 49–54, 2016.

[22] P. Dehghanian and M. Kezunovic, "Probabilistic decision making for the bulk power system optimal topology control," *IEEE Transactions on Smart Grid*, vol. 7, no. 4, pp. 2071–2081, 2016.

[23] D. N. Trakas and N. D. Hatziargyriou, "Optimal distribution system operation for enhancing resilience against wildfires," *IEEE Transactions on Power Systems*, vol. 33, no. 2, pp. 2260–2271, 2017.

[24] Q. Nie, X. Qian, S. Guo, S. Jones, M. Doustmohammadi, and M. D. Anderson, "Impact of COVID-19 on paratransit operators and riders: A case study of central Alabama," *Transportation research part A: policy and practice*, vol. 161, pp. 48–67, 2022.

[25] Y. Dong, W. Zheng, X. Cao, X. Sun, and Z. He, "Co-planning of hydrogen-based microgrids and fuel-cell bus operation centers under low-carbon and resilience considerations," *Applied Energy*, vol. 336, p. 120849, 2023.

[26] U.S. Environmental Protection Agency, "Emission factors for greenhouse gas inventories." https://www.epa.gov/sites/default/files/2018-03/documents/emission-factors_mar_2018_0.pdf, 2018.